



## RESEARCH ARTICLE

10.1029/2021GC009868

## Focusing Fluids in Faults: Evidence From Stable Isotopic Studies of Dated Clay-Rich Fault Gouge of the Alberta Rockies

E. A. Lynch<sup>1</sup> , D. Pană<sup>2</sup>, and B. A. van der Pluijm<sup>1</sup> <sup>1</sup>Department of Earth and Environmental Sciences, University of Michigan, Ann Arbor, MI, USA, <sup>2</sup>Alberta Geological Survey, Edmonton, AB, Canada

## Key Points:

- Isotopic makeup of clay fault gouges document Late Mesozoic/Early Cenozoic deformational fluid regimes in the Canadian Cordillera thrust belt
- Pervasive meteoric fluid was present during thrusting, with variable input from deeper metamorphic fluid sources
- Fluid mixing was not dependent on spatial or temporal context in the fold-thrust belt

## Correspondence to:

E. A. Lynch,  
[lynchea@umich.edu](mailto:lynchea@umich.edu)

## Citation:

Lynch, E. A., Pană, D., & van der Pluijm, B. A. (2021). Focusing fluids in faults: Evidence from stable isotopic studies of dated clay-rich fault gouge of the Alberta Rockies. *Geochemistry, Geophysics, Geosystems*, 22, e2021GC009868. <https://doi.org/10.1029/2021GC009868>Received 28 APR 2021  
Accepted 21 OCT 2021

**Abstract** Isotopic studies of Canadian Rocky Mountain thrust faults preserve the timing and identity of orogenic fluids and their fault zone pathways. Using previously dated samples, we measure the O- and H-isotopic compositions of fault gouge. These nearly 100% neomineralized gouges and their associated damage zones act as primary orogenic fluid pathways. As such, they provide a specific and local look into the nature of the Late Jurassic to Early Eocene orogenic plumbing system in the Alberta Rockies. Considering clay polytype stability and regional temperature conditions, we obtain a range of geofluid isotopic compositions during Jurassic-Eocene thrust faulting:  $\delta^{18}\text{O}_{\text{fluid}}$  ranged from  $\sim -3.3$  to  $9.2 \pm 3.2\text{‰}$ ;  $\delta\text{D}_{\text{fluid}}$  ranged from  $-119$  to  $-46 \pm 13\text{‰}$  VSMOW. The range of O- and H-isotopic compositions reflects mixing of fluid sources, including the pervasive presence of surface-sourced fluids (up to  $\sim 90\%$ ). The interpreted prevalence of a surface fluid source in fault rocks is in agreement with regional isotopic trends previously observed in undated veins of fractured host rock. Our results confirm that thrust faults of the Alberta Rocky Mountains acted as major fluid-focusing conduits during orogenic activity. We further show that these faults incorporated both deeply sourced and surface-sourced fluids into zones of enhanced and dynamic permeability, heterogeneously distributing fluids along fault planes across the fold-thrust belt, promoting the growth of fault-zone weakening clay minerals.

## 1. Introduction

Until the past few decades, the study of ancient, orogenic, shallow-crustal fluids has relied primarily on veins and fluid inclusions. These studies have identified surface (meteoric and basinal) fluids as a main component of vein-forming fluids, though deeply sourced metamorphic and magmatic fluids were also considered (e.g. Anastasio et al., 2004; Bebout et al., 2001; Cooley et al., 2011; Evans & Battles, 1999; Evans et al., 2012; Kirschner & Kennedy, 2001; Rygel et al., 2006; Travé et al., 2007). Several studies have described the mixing of multiple crustal fluid sources in diverse crustal regimes and in numerous geographic locations (e.g. Cooley et al., 2011; Fitz-Diaz et al., 2014; Menzies et al., 2016; Nesbitt & Muehlenbachs, 1991; Travé et al., 2007). Clay mineral studies are a robust complement to vein studies, since clays contain both structural H and O in their crystal lattice making them favorable for combined isotopic study. As with veins, isotopic studies of deformationally mediated clay minerals, have invariably identified meteoric or surface-sourced fluids (including meteorically derived basinal fluid) as a primary component of geofluids active during deformation (Boles et al., 2015; Fitz-Diaz et al., 2014, 2011; Haines et al., 2016; Lynch et al., 2019; Lynch & van der Pluijm, 2016). The crustal position of clay minerals in fault gouge, allows them to isotopically record the passage and/or presence of tectonic fluids as they mineralize, reducing friction along fault planes and promoting continued deformation.

Faults are generally interpreted as conduits for geofluid flow. The fault valve mechanism, proposed by Sibson (1992) has been cited as a method for transporting significant volumes of water through the brittle crust along structural discontinuities during episodes of fault activity. Both fault slip and fault-related deformation locally affect the permeability structure of the upper crust, providing far-reaching pathways of enhanced permeability surrounding active faults that exponentially decreases as distance from the fault plane increases, and that can vary by two to three orders of magnitude during cyclic deformation (Evans et al., 1997; Faulkner & Armitage, 2013; Faulkner et al., 2010). In this environment, other forces, such as burial pressure/temperature increases act as drivers controlling the geofluid flow vectors (Koons &

© 2021. The Authors.  
This is an open access article under the terms of the [Creative Commons Attribution License](https://creativecommons.org/licenses/by/4.0/), which permits use, distribution and reproduction in any medium, provided the original work is properly cited.

Craw, 1991; Sibson, 1992). Notably, this fluid flow imparts chemical and mineral changes to the surrounding crustal rock, resulting in metasomatism and authigenic mineral growth. These processes leave behind an imprint of the geofluids involved during deformation, providing the opportunity to decipher the variable roles of orogenic fluid sources and their implications on the relative impacts of major fluid-driving forces.

The main sources of fluids in fold-thrust belts are, (a) the infiltration and subsequent expulsion of meteoric and basinal, surface-sourced fluids, and (b) the release and upward flow of deep, magmatic and metamorphic fluids (e.g. Bradbury & Woodwell, 1987; Dworkin, 1999; Fyfe & Kerrich, 1985; Ge & Garven, 1989; Hüpers et al., 2017; Koons & Craw, 1991; Menzies et al., 2014; Walther & Wood, 1984). Distinguishing between them can be done through targeted stable isotopic studies of fluid-grown minerals. The Canadian Rockies provides an ideal location to examine the contribution of deep vs. surface fluids for several reasons. First, at high latitudes and high elevations, surface-derived meteoric waters are isotopically extremely light and, therefore, easily distinguished from other fluid sources by markedly negative hydrogen ( $\delta D$ ) and oxygen ( $\delta^{18}O$ ) isotopic signatures. Deep-sourced metamorphic and/or magmatic sources have considerably higher  $\delta$ -values for hydrogen and oxygen.

However, the direct study of fault fluids has been difficult for several reasons, among them the lack of readily extractable and isolatable mineral phases in fault rock material. Advances in precision shallow fault-dating overcome this particular hurdle, providing insight into the timing of fault activation through  $^{40}Ar/^{39}Ar$ -dating of secondary clay minerals separates that form during fluid flow in active fault zones (e.g., van der Pluijm et al., 2001). Building on the dating of fault-grown mineral studies, this article utilizes previously dated clays from the Alberta Rocky Mountains (Pană & van der Pluijm, 2015) to determine the isotopic composition and source of fluids that were channeled through fault zones during episodic fault slip and regional deformation. Using fault gouge samples as fluid proxies is complementary to vein-based studies, as they provide independent insight into the absolute timing of fluid flow through Ar-dating, and isotopic studies utilize regional temperature constraints gained from fluid inclusion analysis. The application of paired oxygen and hydrogen isotopic analysis of dated clays provides a multi-dimensional picture of the role and location of fault rock fluids in major orogenic settings. This article presents hydrogen and oxygen isotope data from the direct study of dated gouge, clarifying the relationship between regional deformation and localized faulting, associated fluid flow and fluid-driving forces in the southern Canadian Rocky Mountains.

## 2. Regional Geologic Context

Our study area is in the Alberta portion of the southern Canadian Rocky Mountain fold-and-thrust belt (RM-FTB), which is part of the Cordilleran Foreland belt of North America. Westerly from the Foreland belt, the southern Canada Cordillera is traditionally subdivided into the Omineca, Intermontane, Coast, and Insular morphogeological belts (e.g., Gabrielse et al., 1992; Figure 1). The Foreland belt comprises strata of North American origin, the Omineca Belt is the region of overlap between ancestral North America and allochthonous rocks, whereas belts to the west include a collage accreted of allochthonous and autochthonous terranes (e.g., Monger, 1984, 1989; Price, 1986, 1994). The upper-crustal tectonic elements (or allochthonous terranes) were juxtaposed over each other and over the western margin of the North American craton along a system of interleaved, northeast-and southwest-verging major thrust faults (Monger et al., 1982; Struik, 1988; Tempelman-Kluit, 1979).

Although the paleogeography and tectonic models of the southern Canadian Cordillera are somewhat controversial, it is widely accepted that Neoproterozoic rifting of Rodinia led to the onset of Windermere deposition and was followed by seafloor spreading and continental drift in the latest Neoproterozoic. By the earliest Cambrian, a persistent continental shelf-slope system was established between ancient North America and the newly opened ocean, a distant ancestor of the present Pacific Ocean. The paleogeography of the ancient continental margin evolved from a passive margin until Middle Devonian to a mainly convergent plate margin until the present (e.g., Monger, 1984, 1989; Monger & Price, 2002).

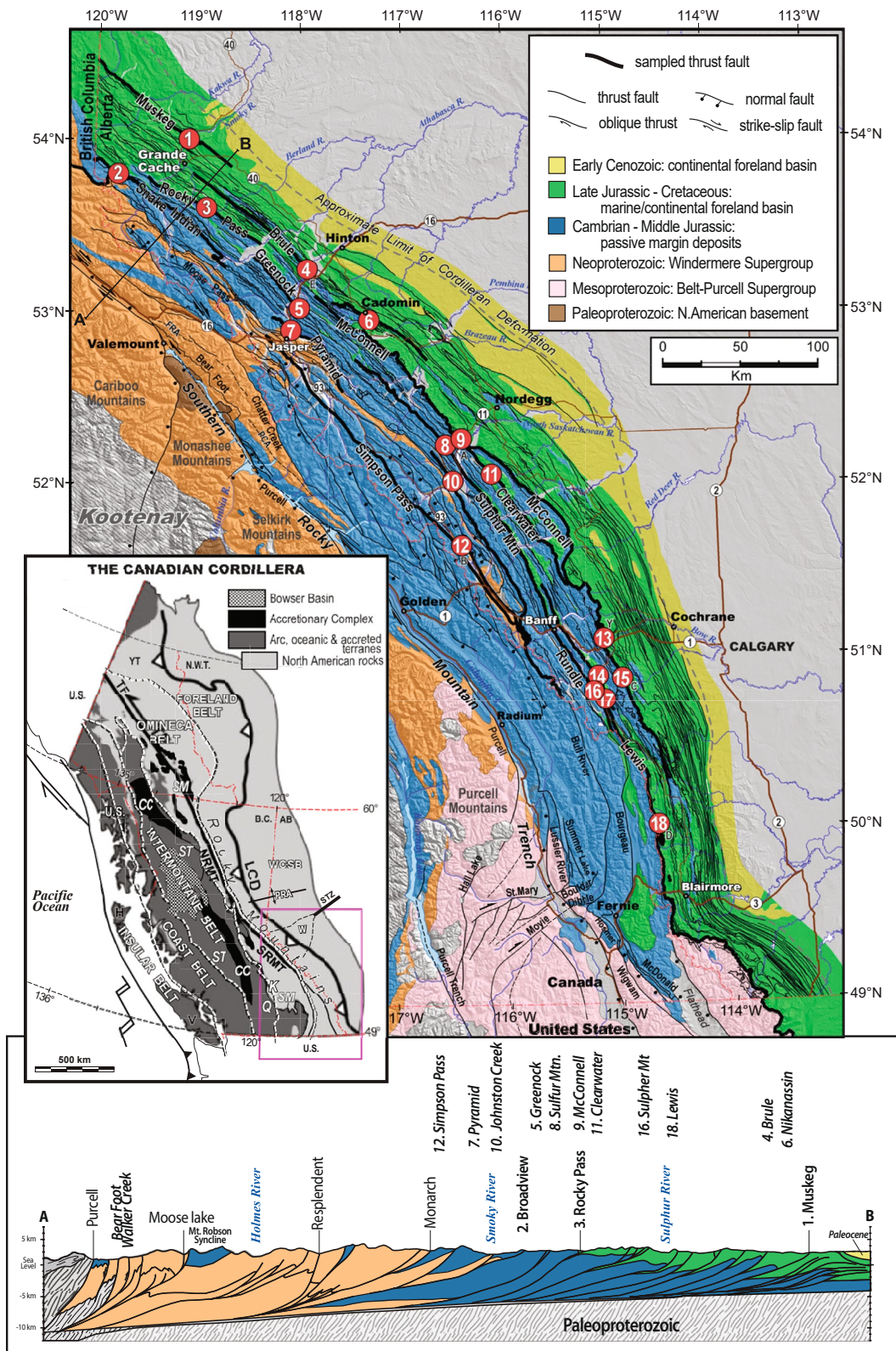


**Figure 1.** Geologic map and cross section after Paná and van der Pluijm (2015). The locations of samples collected from the Canadian Cordillera fold-thrust belt in Alberta are shown on the map and positioned relatively on the cross-section. Italicized thrust names listed on the cross-section do not intersect the section. Sample A (a footwall shale sample) shares the same location (within 300 m) as Sample 9. Samples 13–15 and 17 from Paná and van der Pluijm (2015) were not available for use in this study.

Tectonic events did not markedly affect ancestral North American rocks in Canada until the Middle Jurassic. Events leading to Cordilleran mountain building started in Middle Jurassic time, as a result of breakup of Pangea and North American plate motion toward subduction zones at its western margin, followed by collisions with eastward and northeastward drifting island arcs on the proto-Pacific lithosphere (e.g., Gabrielse et al., 1992; Monger, 1984, 1989; Monger & Price, 2002; Monger et al., 1972, 1982). Between the Middle Jurassic and early Eocene, the Cordilleran realm was mainly under compression, accompanied at different times by sinistral and dextral transpression (e.g., Evenchick et al., 2007; Monger & Gibson, 2019).

The investigated RM-FTB formed as a thin-skinned accretionary wedge in a retroarc tectonic setting between the Middle Jurassic and early Eocene (Monger & Price, 2002; Pană & van der Pluijm, 2015). It is bounded to the east by the elusive eastern limit of Cordilleran deformation, and to the west by the Rocky Mountain trench. The detached and displaced supracrustal rocks comprise several broad tectono-stratigraphic assemblages, mostly of North American origin, deposited within the Western Canada sedimentary basin. The thick stack of east-vergent, generally downward- and eastward-younging thrust slices includes Proterozoic strata, locally overprinted by low-to medium-grade metamorphism, in the western parts of the RM-FTB, unmetamorphosed Paleozoic strata in the central and eastern parts, and Mesozoic to Cenozoic rocks in the frontal parts (Monger, 1989). The southernmost portion of the Canadian RM-FTB also includes strata of the Belt-Purcell Supergroup deposited in a controversial Mesoproterozoic tectonic setting (e.g., Ross & Villeneuve, 2003; Sears & Price, 2003).

### 3. Sample Location and Mineralogy

Fifteen (15) samples analyzed in this study were collected from the eastern, non-metamorphosed portion of the RM-FTB in Alberta, spanning the length of the belt from approximately 50°–54°N latitude (Figure 1, Table 1). Twelve (12) samples of fault gouge and one (1) footwall shale sample were previously dated using Ar geochronology (Pană & van der Pluijm, 2015); two (2) additional fault gouge ages were reported by van der Pluijm et al. (2006). Using the combined illite ages from both studies, Pană and van der Pluijm (2015) identified four major pulses of contractional deformation between the Late Jurassic and Early Eocene, which preceded middle to late Eocene extensional collapse of the orogen. Authigenic illite shows that the growth of fault-related clay minerals occurred in the presence of ancient orogenic fluids, so their stable isotopic makeup reflects the stable isotopic composition of the deformational fluids. Though earlier work determined the polytypes of *illite* present in each gouge sample (required for Ar/Ar-dating), additional work was needed to fully characterize the clay mineralogy in order to extract the relevant isotopic signatures from authigenic illite.

The methods to process samples and characterize illitic materials are described in Pană and van der Pluijm (2015) and van der Pluijm et al. (2006). We completed additional clay mineral X-ray diffraction (XRD) characterization on each of the four <2 μm size fractions through low-angle (2°–40°2θ) scanning of oriented mounts, which were prepared using the suspension method (Moore & Reynolds, 1997). We used a Cu-source Rigaku Ultima IV X-Ray Diffractometer equipped with a Ni foil k-beta filter, scanning at a speed of 1°/minute and a step size of 0.02°2θ. Though illite was the dominant clay mineralogy for all samples, we also identified the presence of minor quartz, calcite, kaolinite, and chlorite in some of the samples (Figure 2). DP10-1 (Sample 7) also contained a trace amount of gypsum. Using the mineral reference intensities (MRI) method (Moore & Reynolds, 1997), we quantify the proportions of clay minerals present in each sample (Table 2).

### 4. Stable Isotopic Composition of Clay Gouge

#### 4.1. Isotopic Measurement

Stable isotopic measurements of hydrogen and oxygen were completed at the Institute of Earth Surface Dynamics (IDYST) at the University of Lausanne (UNIL). Approximately 1.5–2 mg of duplicate sample separates were encapsulated in silver foil packets and kept under vacuum for at least 12 hr prior to analysis. Samples were then quickly transferred to a helium-flushed zero-blank autosampler connected

**Table 1**  
Sample Locations and Descriptions

Sample ID	Fault	Hanging wall	Foot wall	Latitude	Longitude
1. DP10-406C	Muskeg Thrust	Gates sandstone <i>Lower Cretaceous</i>	Kaskapau shale/siltstone <i>Upper Cretaceous</i>	54° 1' 21.0" N	119° 3' 36.7" W
2. DP11-90	Broadview (Snake Indian) Thrust	Whitehorse silty dolomite <i>Triassic</i>	Fernie shale <i>Jurassic</i>	53° 48' 47.7" N	119° 44' 48.7" W
3. DP11-100	Rocky Pass Thrust	Rundle carbonate <i>Mississippian</i>	Nikanassin shale/siltstone <i>U.Jurassic – L.Cretaceous</i>	53° 37' 22.9" N	118° 52' 18.7" W
4. DP10-166D	Brule Thrust	Palliser carbonate <i>Upper Devonian</i>	Nikanassin shale/siltstone <i>U.Jurassic – L.Cretaceous</i>	53° 16' 49.8" N	117° 53' 21.8" W
5. DP10-140A	Greenock Thrust	Lower Rundle carbonate <i>Mississippian</i>	Fernie shale <i>Jurassic</i>	53° 3' 14.0" N	117° 58' 4.1" W
6. DP10-11	Nikanassin Thrust	Palliser carbonate <i>Upper Devonian</i>	Nikanassin shale/siltstone <i>U.Jurassic – L.Cretaceous</i>	53° 0' 16.3" N	117° 18' 47.4" W
7. DP10-1	Pyramid Thrust (Jasper)	Miette grit <i>Neoproterozoic</i>	Perdix/Sassenach shale <i>Upper Devonian</i>	52° 55' 4.8" N	118° 3' 11.9" W
8. DP11-104	Sulfur Mt. Thrust (Abraham Lake)	Rundle carbonate <i>Mississippian</i>	Fernie shale <i>Jurassic</i>	52° 16' 36.8" N	116° 34' 58.4" W
9. DP10-2	McConnell Thrust (Abraham Lake)	Eldon carbonate <i>Middle Cambrian</i>	Luscar shale/siltstone <i>Lower Cretaceous</i>	52° 16' 10.7" N	116° 23' 35.7" W
10. DP11-107	Johnston Creek Thrust	Miette sand/siltstone, grit <i>Neoproterozoic</i>	Eldon carbonate <i>Middle Cambrian</i>	52° 3' 9.2" N	116° 30' 16.7" W
11. DP11-114	Clearwater Thrust	Banff carbonate <i>Mississippian</i>	Kootenay shale/siltstone <i>U.Jurassic – L.Cretaceous</i>	52° 3' 19.1" N	116° 4' 31.1" W
12. DP11-112	Simpson Pass Thrust	Gog qtzite/qtz sandstone <i>Lower Cambrian</i>	Pika carbonate <i>Middle Cambrian</i>	51° 41' 35.6" N	116° 25' 10.9" W
16. KKF-91-1A	Sulfur Mt. Thrust (Kananaskis)	Palliser carbonate <i>U. Devonian</i>	Fernie shale <i>Jurassic</i>	50° 53' 59.8" N	114° 56' 33.8" W
18. KKF-102E	Lewis Thrust (Gould Dome)	Palliser carbonate <i>U. Devonian</i>	Belly River shale/siltstone <i>Upper Cretaceous</i>	50° 2' 6.9" N	114° 38' 42.5" W
A. MTF-FW2	McConnell Footwall shale sample	–	Luscar shale/siltstone <i>Lower Cretaceous</i>	52° 16' 10.7" N	116° 23' 35.7" W

to a Thermo Finnigan Delta Plus XL thermochemical elemental analyzer (TC/EA). A helium carrier gas transferred the reduced hydrogen gas to the mass spectrometer, which measured the ratios of H<sub>2</sub> and DH gases, and the weight percent water for each sample. Results are reported using  $\delta$ -notation relative to standard mean ocean water (SMOW) and are reproducible to  $\pm 3\%$  across duplicate sample aliquots.

Prior to oxygen analyses, samples were loaded onto a platinum sample plate and heated in an oven at 150°C for at least 12 hr. Oxygen gas was isolated from silicate samples for isotopic measurements with laser fluorination (e.g., Sharp, 1990), using a vacuum of approximately 10<sup>-4</sup> Pa prior to fluorination. Extracted oxygen gas was collected on a zeolite molecular sieve and transferred to a Finnigan MAT 253 Mass Spectrometer for measurement. As with hydrogen, results are reported using  $\delta$ -notation relative to SMOW and

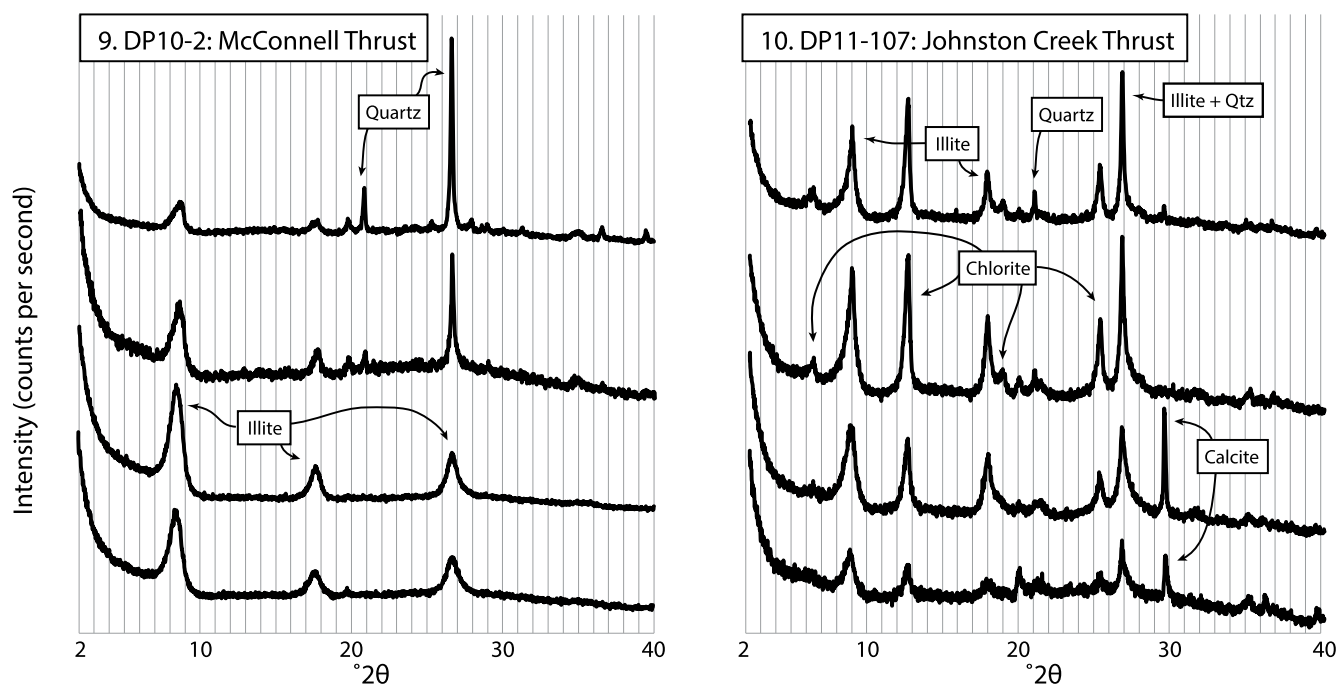


**Figure 2.** Two representative series of oriented XRD patterns. In both diagrams, the coarsest fraction is on the top, the finest fraction on the bottom. The left patterns (DP10-2) are representative of the several samples whose clay mineralogy contain only illite. The right patterns (DP11-107) are more representative of samples that have two clay minerals present, in this case, illite and chlorite. Both samples also indicate the presence of quartz, particularly in the coarser fractions (peaks at  $20.8^\circ$  and  $26.5^\circ 2\theta$ ). The right sample also shows evidence of calcite, present in the two finer fractions (peak at  $29.4^\circ 2\theta$ ).

are reproducible to  $\pm 0.2\%$ . We were unable to measure one sample (16: KKF-91-1A) for oxygen isotopic composition due to its reaction with  $F_2$  gas at room temperature.

#### 4.2. Hydrogen Isotopic Results

Two aliquots of each sample size fraction were measured for hydrogen isotopic composition. In nearly all cases, measurements are reproducible to  $\leq 3\%$ , with the maximum error on duplicate measurements of  $3.7\%$  (sample 12: DP11-112MC) (Table 3).

A York-style bivariate linear regression analysis of hydrogen isotopic compositions and authigenic ( $1M_d$ ) illite quantifications allows the extrapolation to 100% authigenic material and therefore, the determination of the hydrogen isotopic composition of deformation-related illite of the gouge (Table 4; Boles et al., 2015; Lynch et al., 2019; Lynch & van der Pluijm, 2016; York, 1968). During the preparation of one sample (sample 4: DP10-166D, Brule Thrust), hydrogen-rich organic material was concentrated by centrifugation into the fine fraction, which we discard to obtain a regression value of  $-136.5 \pm 22.4\%$   $\delta D$ .

#### 4.3. Oxygen Isotopic Results

Oxygen measurements were completed for the finest fraction of each sample. Unlike hydrogen, oxygen isotopic values are not affected by the presence of hydrocarbons that may concentrate into the finer fractions. Instead, oxygen isotopic values are affected by the presence of other rock-forming minerals, including silicates, oxides, and carbonates. Non-clay silicate minerals are absent in any of the finest fractions, except trace amounts of quartz and gypsum in sample 7 (DP10-1). Minor ( $< 5$  wt%) calcite was removed prior to oxygen isotopic analysis by reaction with 10% HCl (Table 4). The variable presence of the  $2M_1$ , high-temperature detrital illite polymorph, which was seen in the fine fractions in concentrations up to  $18\% \pm 2\%$  (Lewis Thrust, sample 18), with an average of  $8\% \pm 2\%$ , is an irreducible source of error. Though we are unable to

**Table 2**  
*Mineralogy of Samples*

Sample ID	Size fraction	MRI quantification			Illite polytype <sup>a</sup>			Non-clay minerals
		%Chl	%Kaol	%Ill	%2M1	%1Md	%1Md/clay	
1. DP10-406C	C	—	—	63	21	79	50	Qtz
<i>Muskeg Thrust</i>	MC	—	—	77	16	84	35	Qtz
	M	—	—	96	10	90	14	Qtz
	F	—	—	100	6	94	6	—
	C	—	—	90	19	81	27	Qtz
2. DP11-90	C	—	—	90	19	81	27	Qtz
<i>Broadview (Snake Indian) Thrust</i>	MC	—	—	95	14	86	18	?
	M	—	—	100	9	91	9	Cct
	F	—	—	100	5	95	5	Cct
3. DP11-100	C	—	—	100	36	64	36	Qtz, Cct
<i>Rocky Pass Thrust</i>	MC	—	—	100	26	74	26	Cct
	M	—	—	100	17	83	17	Cct
	F	—	—	100	13	87	13	Cct
	C	—	—	100	24	76	24	Qtz
4. DP10-166D	C	—	—	100	24	76	24	Qtz
<i>Brule Thrust</i>	MC	—	—	100	18	82	18	Qtz
	M	—	—	100	11	89	11	—
	F	—	—	100	6	94	6	—
	C	—	—	100	32	68	68	Qtz
5. DP10-140A	C	—	—	100	32	68	68	Qtz
<i>Greenock Thrust</i>	MC	—	—	100	30	70	70	Qtz (tr)
	M	—	—	100	9	91	91	—
	F	—	—	100	2	98	98	—
	C <sup>b</sup>	?	?	?	38	62	62 <sup>b</sup>	?
6. DP10-11	C <sup>b</sup>	?	?	?	38	62	62 <sup>b</sup>	?
<i>Nikanassin Thrust</i>	MC <sup>c</sup>	?	?	?	19	81	81 <sup>c</sup>	?
	M	—	—	100	11	89	89	—
	F	—	—	100	6	94	94	—
7. DP10-1	C	—	—	100	28	72	7	Qtz
<i>Pyramid Thrust (Jasper)</i>	M	—	—	100	16	84	84	Qtz
	F	—	—	100	11	89	89	Qtz, Gyp
	C	23	—	77	42	58	55	Qtz, Cct
8. DP11-104	C	23	—	77	42	58	55	Qtz, Cct
<i>Sulfur Mt. Thrust (Abraham Lake)</i>	MC	17	—	83	29	71	41	Qtz, Cct
	M	5	—	95	11	89	15	Cct
	F	—	—	100	7	93	7	Cct (tr)
	C	—	—	100	20	80	80	Qtz
9. DP10-2	C	—	—	100	20	80	80	Qtz
<i>McConnell Thrust (Abraham Lake)</i>	MC	—	—	100	16	84	84	Qtz
	M	—	—	100	8	92	92	—
	F	—	—	100	6	94	94	—
	C	29	—	71	41	59	58	Qtz
10. DP11-107	C	29	—	71	41	59	58	Qtz
<i>Johnston Creek Thrust</i>	MC	24	—	76	31	69	48	Qtz
	M	14	—	86	22	78	33	Cct
	F	18	—	82	11	89	27	Cct
	C	—	—	100	32	68	68	Qtz
11. DP11-114	C	—	—	100	32	68	68	Qtz

(Continued)

**Table 2**  
Continued

Sample ID	Size fraction	MRI quantification			Illite polytype <sup>a</sup>			Non-clay minerals
		%Chl	%Kaol	%Ill	%2M1	%1Md	%1Md/clay	
<i>Clearwater Thrust</i>	MC	—	—	100	18	82	82	Qtz
	M	—	—	100	11	89	89	—
	F	—	—	100	8	92	92	—
12. DP11-112	C	12	—	88	52	48	58	Qtz
<i>Simpson Pass Thrust</i>	MC	7	—	93	33	67	38	—
	M	6	—	94	11	89	16	—
	F	—	—	100	7	93	7	Cct
16.KKF-91-1A								
<i>Sulfur Mt. Thrust (Kananaskis)</i>	C	—	—	100	30	70	70	Qtz
	M	—	—	100	5	95	95	—
	F	—	—	100	5	95	95	—
18. KKF-102E	C	—	57	43	73	27	12	Qtz
<i>Lewis Thrust (Gould Dome)</i>	M	—	30	70	39	61	43	—
	F	—	5	95	18	82	78	—
A. MTF-FW2	C	—	—	100	32	68	68	Qtz
<i>McConnell Footwall Shale</i>	M	—	—	100	8	92	92	—
	F	—	—	100	6	94	94	—

Note. tr, trace.

<sup>a</sup>From Paná and van der Pluijm (2015). <sup>b</sup>No oriented sample available. <sup>c</sup>Clay minerals not identifiable in oriented samples.

separate the authigenic from detrital illite in the finest fraction, we use the  $\delta O_{\text{fine}}$  values as representative of near-authigenic values. We find no systematic variation between the percentage of detrital illite and the  $\delta O_{\text{fine}}$  values.

## 5. Discussion

### 5.1. Fractionation Temperature Constraints

With constraints on fractionation temperature, the isotopic composition of mineralizing fluids is calculated from the isotopic composition of authigenic clay. Fractionation temperatures are constrained by the minimum formation temperature of 1Md illite,  $\sim 90^{\circ}\text{C}$  (e.g., Haines & van der Pluijm, 2012). Maximum fractionation temperatures are obtained from mineralogic and other geologic evidence. A geothermal gradient of  $\sim 20\text{--}25^{\circ}\text{C}/\text{km}$  has been estimated for the Canadian Rocky Mountain foreland fold-thrust belt region (e.g. England & Bustin, 1986; Hardebol et al., 2009; Osadetz et al., 2004). With a maximum thickness of  $\sim 8$  km for the deformed foreland wedge (Paná & Elgr, 2013; Price, 1981), this equates to temperatures less than  $160^{\circ}\text{C}\text{--}200^{\circ}\text{C}$ . Additionally, Nesbitt and Muehlenbachs (1995) recorded fluid inclusion homogenization temperatures in calcite veins from the fold and thrust belt to be between  $120^{\circ}\text{C}$  and  $200^{\circ}\text{C}$ . These observations, along with maximum temperature estimates from organic maturity indicators (England & Bustin, 1986; Hardebol et al., 2009; Kalkreuth & McMechan, 1984) and conodont alteration indices (Symons & Cioppa, 2002) characterize the thermal history of the fold-thrust belt and suggest that the viable temperature range during deformation was  $100^{\circ}\text{C}\text{--}200^{\circ}\text{C}$ . Since many of the exhumed thrusts likely formed at shallower depths and, noting that the upper stability of low-temperature 1Md illite of  $\sim 180^{\circ}\text{C}$  (Haines & van der Pluijm, 2012), we use an upper temperature of fault rock illite of  $180^{\circ}\text{C}$ , reflecting absolute maximum thrusting and fault rock formation at 7–8 kilometers depth.



**Table 3**  
*Hydrogen Isotopic Results*

Sample ID	Size fraction	$\delta D$ (‰)	Dupl. (‰)	Sample ID	Size fraction	$\delta D$ (‰)	Dupl. (‰)
1. DP10-406C	C	-83.5	-84.1	8. DP11-104	C	-101.7	-101.7
<i>Muskeg Thrust</i>	MC	-74.6	-75.6	<i>Sulfur Mt. Thrust (Abraham Lake)</i>	MC	-100.1	-100.3
	M	-94.4	-96.4		M	-86.8	-86.9
	F	-101.9	-101		F	-73.8	-73.9
2. DP11-90	C	-71.1	-72.7	9. DP10-2	C	-110.7	-111.8
<i>Broadview (Snake Indian) Thrust</i>	MC	-69.2	-71.1	<i>McConnell Thrust (Abraham Lake)</i>	MC	-107.6	-110.8
	M	-64	-65.6		M	-92.5	-90.6
	F	-66.4	-65.8		F	-89.4	-87.6
3. DP11-100	C	-121.4	120.5	10. DP11-107	C	-80.4	-79.5
<i>Rocky Pass Thrust</i>	MC	-118.8	-118.3	<i>Johnston Creek Thrust</i>	MC	-95	-94.8
	M	-102	-101.6		M	-97.2	-96.4
	F	-95.8	-97		F	-89.5	-89
4. DP10-166D	C	-73.6	-73.9	11. DP11-114	C	-116.8	-118.2
<i>Brule Thrust</i>	MC	-98.8	-98.1	<i>Clearwater Thrust</i>	MC	-125.9	-125
	M	-97.3	-97.4		M	-118.9	-116.6
	F <sup>a</sup>	-42.6	-44.6		F	-108	-108.3
5. DP10-140A	C	-94.2	-95	12. DP11-112	C	-115.5	-114.1
<i>Greenock Thrust</i>	MC	-98.2	-95.6	<i>Simpson Pass Thrust</i>	MC	-112.9	-115
	M	-102.6	-102.4		M	-120.4	-116.7
	F	-78.4	-78.5		F	-98.2	-96
6. DP10-11	C	-112.2	-114.7	16. KKF-91-1A			
<i>Nikanassin Thrust</i>	MC	-114.9	-115.1	<i>Sulfur Mt. Thrust (Kananaskis)</i>	C	-119.1	-120.4
	M	-104.4	-103.9		M	-106.5	-107.1
	F	-107	-103.9		F	-116.3	-116.1
7. DP10-1	C	-105.7	-105.5	18. KKF-102E	C	-127.9	-129.8
<i>Pyramid Thrust (Jasper)</i>	M	-81.9	-81.8	<i>Lewis Thrust (Gould Dome)</i>	M	-124.3	-124
	F	-49.2	-51.1		F	-115.9	-114.1
				A. MTF-FW2	C	-117.2	-118.5
				<i>McConnell Footwall Shale</i>	M	-95.2	-95.4
					F	-102.7	-100.8

<sup>a</sup>Organic-rich sample.

## 5.2. Characteristics and Identity of Mineralizing Fluid

We calculate the composition of the fluid isotopic values for a large temperature window to capture any uncertainty related to local variations in geothermal gradient and fluid-mediated heat exchange along the faults. Water composition was calculated using the fractionation equations of Capuano (1992) and Sheppard and Gilg (1996) for O and H respectively (Table 5, Figure 3). The range of results produced show a broad overlap between mineralizing fluids and Alberta Basin fluids (Connolly et al., 1990; Hitchon & Friedman, 1969; Sheppard, 1986), regardless of the temperature used for the fractionation calculation. On the higher end of the temperature range, fluids have slightly more positive  $\delta^{18}O$  values and more negative  $\delta D$  values. This would imply more water-rock interaction and oxygen buffering (smaller water/rock ratio and/or longer fluid travel pathways through the fold thrust belt). However, the presence of very light hydrogen requires a high latitude or high elevation meteoric fluid as

**Table 4**  
*Isotopic Composition of Authigenic Illite*

Sample ID	Fault/Description	$\delta D_{\text{authigenic}}$	$\delta O_{\text{fine}} (\pm 2\text{‰})$
1. DP10-406C	Muskeg Thrust	$-105.7 \pm 2.9\text{‰}$	12.0‰
2. DP11-90	Broadview (Snake Indian) Thrust	$-63.1 \pm 2.0\text{‰}$	19.3‰
3. DP11-100	Rocky Pass Thrust	$-80.8 \pm 6.8\text{‰}$	20.3‰
4. DP10-166D	Brule Thrust	$35.4 \pm 72.1\text{‰}^{\text{a}}$ $-136.5 \pm 22.4\text{‰}^{\text{b}}$	14.6‰
5. DP10-140A	Greenock Thrust	$-71.9 \pm 7.3\text{‰}$	17.1‰
6. DP10-11	Nikanassin Thrust	$-102.1 \pm 2.3\text{‰}$	14.6‰
7. DP10-1	Pyramid Thrust (Jasper)	$-17.8 \pm 19.9\text{‰}$	9.4‰
8. DP11-104	Sulfur Mt. Thrust (Abraham Lake)	$-73.1 \pm 2.4\text{‰}$	16.5‰
9. DP10-2	McConnell Thrust (Abraham Lake)	$-77.3 \pm 8.1\text{‰}$	11.4‰
10. DP11-107	Johnston Creek Thrust	$-117.6 \pm 8.6\text{‰}$	11.6‰
11. DP11-114	Clearwater Thrust	$-96.5 \pm 11.7\text{‰}$	10.7‰
12. DP11-112	Simpson Pass Thrust	$-96.9 \pm 4.3\text{‰}$	7.0‰
16. KKF-91-1A	Sulfur Mt. Thrust (Kananaskis)	$-107.7 \pm 2.5\text{‰}$	–
18. KKF-102E	Lewis Thrust (Gould Dome)	$-110.8 \pm 2.1\text{‰}$	8.3‰, 8.1‰ <sup>c</sup>
A. MTF-FW2	McConnell Footwall Shale	$-92.1 \pm 3.3\text{‰}$	13.5‰, 13.3‰ <sup>c</sup>

<sup>a</sup>Using all size fractions. <sup>b</sup>Without fine fraction. <sup>c</sup>Duplicate.

an original fluid source. One sample (sample 7: DP10-1) yields a fluid composition that very closely resembles the isotopic composition of seawater, suggesting that isolated pockets of connate seawater may have persisted locally prior to their expulsion along thrust faults. Several of the calculated isotopic fluid values overlap with the magmatic/metamorphic field, illustrating that though meteoric fluids are a major component in geofluids in many of the fault zones, deeper fluids likely also play a role in deformation. The range in isotopic values of mineralizing fluids shows no systematic temporal or spatial pattern, indicating that fluid regimes did not vary with the timing of orogenic pulse activity nor along orogenic trend (Figure 4).

### 5.3. Percentage Approximations of Fluid Mixing

To allow for discussion of fluid regimes, we simplify major crustal fluid sources into two bins: surface-sourced and deeply sourced. Surface sources include meteoric fluids and meteorically charged, relatively unevolved basinal fluids. Deep sources include magmatic, metamorphic, and highly evolved (high-temperature) basinal fluids. We assume that these ideal end-member fluids were homogeneous through time and space, and that the illitic clay material crystallized at constant temperatures, and under equilibrium fractionation conditions. This is a large oversimplification and is not intended to result in precise measurements or calculations. Instead, we use this platform to spark a discussion around the heterogeneity that is observed in the samples through the lens of two ideal, end-member fluids. With this caveat, we present two fluids for consideration, which we refer to as “surface-sourced” and “deeply sourced” throughout the following discussion.

In order to define our surface-sourced end member, we applied a least squares regression to the data described in Table 5 (excluding the outlying sample 7, which was the only sample containing gypsum, and whose fluid equivalent closely resembles SMOW) for both the maximum and minimum temperature

**Table 5**  
Isotopic Composition of Fault Fluids

Sample ID	Hydrogen ( $\delta D$ ‰)		Oxygen ( $\delta^{18}O$ ‰)	
	90°C (min)	180°C (max)	90°C	180°C
1. DP10-406C	-76	-101	-2.4	4.1
2. DP11-90	-33	-58	4.9	11.4
3. DP11-100	-51	-76	6	12.4
4. DP10-166D	-106	-131	0.2	6.7
5. DP10-140A	-42	-67	2.7	9.2
6. DP10-11	-72	-97	0.2	6.7
7. DP10-1 <sup>a</sup>	12	-13	-5	1.5
8. DP11-104	-43	-68	2.2	8.6
9. DP10-2	-47	-72	-3	3.5
10. DP11-107	-88	-112	-2.8	3.7
11. DP11-114	-66	-91	-3.7	2.8
12. DP11-112	-67	-92	-7.4	-0.9
16. KKF-91-1A	-78	-102	-	-
18. KKF-102E	-81	-106	-6.1, -6.3	0.4, 0.2
A. MTF-FW2	-63	-88	-0.9, -1.1	5.6, 5.4
Average	-66	-90	-1.2	5.3
Minimum	-78 ± 13	-131	2.1 ± 3.3	-0.9
Maximum	-119 ± 13	-58	-4.2 ± 3.3	12.4
	-46 ± 13		9.2 ± 3.3	

<sup>a</sup>Outlier: not included in average, minimum, and maximum.

constraints (Figure 5; Lynch & van der Pluijm, 2021). We extrapolate these regression lines to the intersection with the global meteoric water line ( $\delta D = 8 * \delta^{18}O + 10$ ‰) (Sheppard, 1986). Fractionation at 90°C corresponds to a meteoric fluid with the isotopic signature of  $-13.5$ ‰  $\delta^{18}O$  and  $-98$ ‰  $\delta D$ ; fractionation at 180°C corresponds to a meteoric fluid with the isotopic signature of  $-21.0$ ‰  $\delta^{18}O$  and  $-158$ ‰  $\delta D$ . These intersection points constrain the composition of the meteoric fluid input during fault activity, notably overlapping with penecontemporaneous surface fluids (Bowen & Revenaugh, 2003; Chamberlain et al., 2012; Longstaffe & Ayalon, 1990). The close correlation between the derived isotopic composition of surface fluids and the end-member meteoric fluid composition from fault gouge clays confirms that ancient meteoric fluids were a likely major fluid source in the evolving fold-thrust belt, variably mixing with heavier fluids (Figure 5). For our ideal surface-sourced fluid end member approximation, we define  $\delta D_{\text{surface}}$  as  $-128$ ‰ and  $\delta^{18}O_{\text{surface}}$  as  $-15$ ‰.

Previous studies emphasized the role of migrating, hot, metamorphic fluids during orogenesis (Cooley et al., 2011; Machel & Cavell, 1999; Nesbitt & Muehlenbachs, 1989). Because hydrogen isotopic signatures preserve the original fluid source—as they are not easily reset by water-rock interaction—we use fluid  $\delta D$  values from this study to estimate the relative proportions of end-member fluid input into fault zones. Based on the  $\delta D$  values of fluid inclusions and hydrous silicates in veins collected from greenschist facies in the fold-thrust belt—as high as  $-20$ ‰—Nesbitt and Muehlenbachs (1989) suggested that most fluids involved in the Rocky Mountain thrusting originated from metamorphic devolatilization. Using this end-member  $\delta D$  values as representative of deeply sourced water ( $\delta D_{\text{deep}} = -20$ ‰) and the midpoint of our calculated MWL intersections as representative of meteoric water ( $\delta D_{\text{surface}} = -128$ ‰), we estimate the relative proportion of each fluid source. The average of our calculated fluid  $\delta D$  values ( $-78 \pm 12$ ‰, Table 5) would result from an approximately equal mixture of deeply sourced and surface-sourced fluids (46%/54%), whereas the minimum

fluid value ( $\delta D = -119 \pm 13$ ‰) is just over 90% surface derived, and the maximum ( $\delta D = -46 \pm 13$ ‰) from a 76%/24% deep/surface fluid mixture. The observed range of values indicates that mixing of fluid was not constant through time and space.

#### 5.4. Implications for Ancient Fluid Flow in the Canadian Rockies

The presence of both deeply sourced and surface-sourced fluids in Rocky Mountain thrust faults allows us to explore the relative roles of fluid driving forces during deformation. The prevalence of surface fluids in the Canadian Rockies suggests that gravity—topographic head—is an important fluid driving force that promotes downward penetration of surface-sourced fluids across the mountain belts and foreland basins. This phenomenon has been proposed to explain meteoric isotopic signatures found in fluids of the Alpine fault of New Zealand, a major continental transform boundary (Koons & Craw, 1991; Menzies et al., 2014, 2016) and various low-angle normal faults of the US southwest (Haines et al., 2016). Despite the seemingly unfavorable stress regime, gravity-driven downward penetration of surface fluids through the upper crust is likely a dominant fluid driver in compressional belts as well.

At the same time that deforming fold-thrust belts allow gravity-driven downward fluid penetration, they also present pathways for deeply sourced, hot, high-pressure fluid to be expelled to the surface in response to buoyancy and compressional forces. During continued orogenesis, one might expect

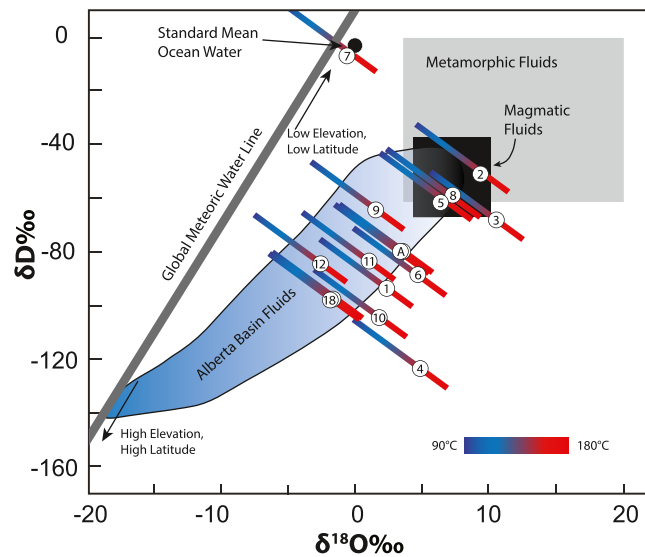


**Figure 3.** Plot of isotopic composition of samples, mineralizing fluids, and major crustal fluid reservoirs. Each calculated fluid composition is shown as a blue-red (left-right) colored bar representing the range of possible  $\delta D$  and  $\delta^{18}O$  values over the 90°C–180°C fractionation temperature range. Each fluid bar is labeled with a number in a small white circle, corresponding to sample numbers that were reported in Table 5. Major fluid reservoirs shown include metamorphic fluids (gray box), magmatic fluids (black box), Alberta/West Canada sedimentary basin fluids (blue shaded region), meteoric water (dark gray line) and standard mean ocean water (SMOW, black circle; Connolly et al., 1990; Hitchon & Friedman, 1969; Sheppard, 1986). Calculated fluid values largely overlap with basin fluids and partly with metamorphic/magmatic fluids. One fluid value corresponds with ocean water isotopic composition.

metamorphic fluid expulsion to peak during peak deformation, perhaps coinciding with the major deformation pulses described by Paná and van der Pluijm (2015). If this were the case, we would expect the earliest fault fluids to be dominated by surface sources, peak deformation to be accompanied by increased metamorphic/magmatic fluid release, and late stage orogenesis to be again dominated by surface-fluids. Looking at Figure 4a, we are tempted to conclude that this is the case for  $\delta^{18}O$ —oldest and youngest fluids, which seem to be more negative (similar to surface-sourced fluids), whereas those in the middle of the age range seem less negative (similar to metamorphic fluids). However, Figure 4b does not show the same pattern for  $\delta D$ , and considering our uncertainties the data does not permit us to take such a bold stand. Interestingly, Nesbitt and Muehlenbachs (1994) did observe a predominance of likely meteoric fluids in their study of postorogenic veins, implying that deep-sourced fluids were not available for mineralization while deformation had nearly ceased. This could also have been due to the fact that the sampled veins were not long-lived conduits for flow, as the thrust faults likely were.

Regardless, though we find isotopic evidence for the involvement of deeply sourced fluids in the RM-FTB, we do not see any clear pattern in the isotopic composition of these fluids that can be easily attributed to either systematically changing fluid inputs or different source compositions through time or during orogenic pulses (Figure 4). Instead, the relative contribution of these deep fluids and surface fluids appears to be heterogeneous through time and across the mountain belt. This suggests one of two things: that local heterogeneities in stress regime and rock fracturing may be a driving factor promoting local to regional scale fluid infiltration to fault-depths, and/or that deeply sourced fluids are not released en masse during progressive deformation. As the two (or more) fluids migrate and mingle, they find crustal weaknesses in the thrust faults and promote new mineral growth therein, including friction-reducing clays. A more thorough sampling campaign, one that combines fault gouge studies with vein studies from the same outcrops, and places them in temperature-depth context on a palinspastically restored cross-section may, in the future, be able to further eliminate uncertainties in this study and continue to unlock the fluid mixing puzzle in fold-thrust belts.

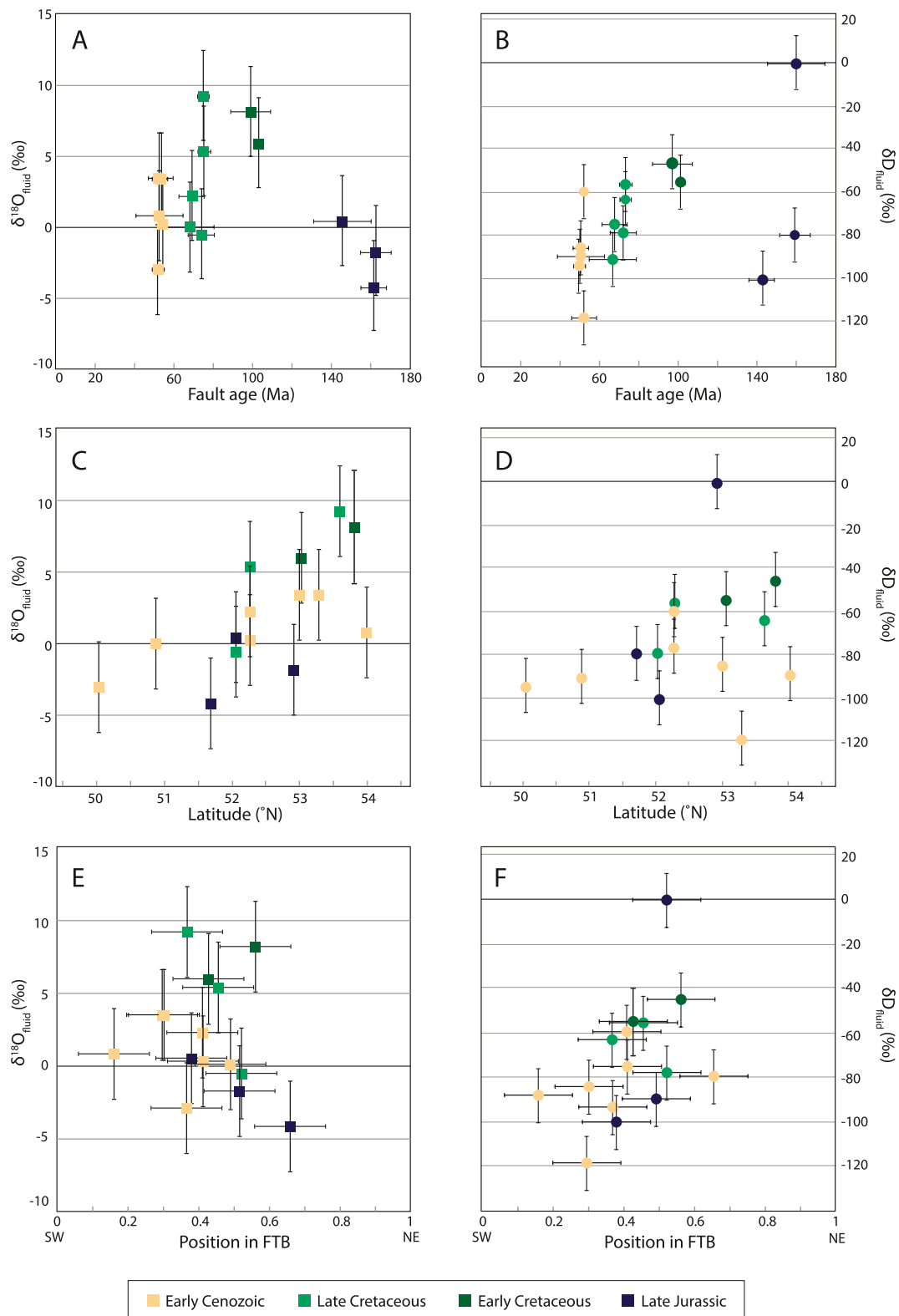
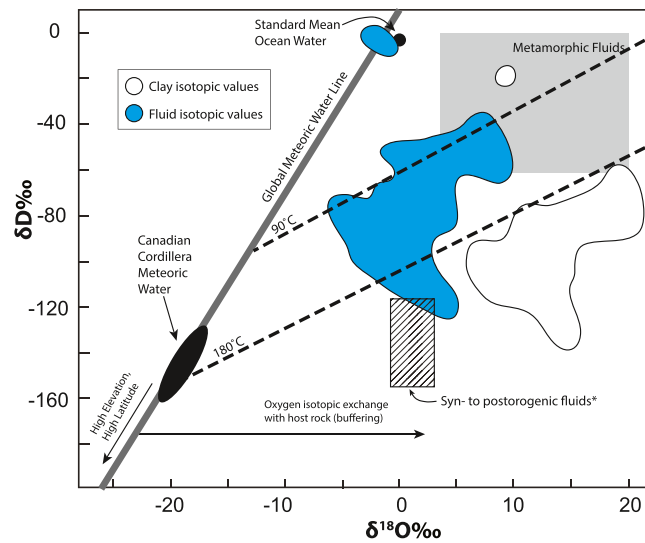


Figure 4.



**Figure 5.** Schematic representation of the isotopic composition of fluids in the Alberta fold-thrust belt. Clay measurements from this study are encompassed by the white outlined region; the calculated mineralizing fluid compositions by the blue outlined region. The results of our least squares regression for fractionation temperature range define the window of likely meteoric fluid compositions between where the dotted regression lines intersect the global Meteoric Water Line. This window overlaps with the  $\delta D$  and  $\delta^{18}O$  values of modern Canadian Cordillera meteoric fluid (Bowen & Revenaugh, 2003; Longstaffe & Ayalon, 1990), which is shown as a black oval, and considered to be one of the end-member mixing fluids. It is likely that during orogenic activity, local meteoric waters would have been less negative than they are today, due both to the lower elevation and lower latitude during the early stages of mountain building. The stippled gray box shows the region of syn- to postorogenic fluids (Nesbitt & Muehlenbachs, 1994) interpreted from fluids inclusions in dolomite veins, which have a slight overlap with clay mineralizing fluids.

## 6. Conclusions

Newly formed clays in fault rock that are found along major thrust faults in the Alberta Rockies allow us to determine the ancient sources and pathways of orogenic fluids during shallow crustal deformation. We examined fault fluids through isotopic analysis of secondarily formed, fault-grown, dated clays in fault gouge and explored the degree of fluid mixing in fault zones. Vein-based studies in older host rock have variably identified metamorphic fluid as a significant contributor during compressional deformation (Cooley et al., 2011; Machel & Cavell, 1999; Nesbitt & Muehlenbachs, 1991, 1994), whereas our study of fault gouge shows that surface-sourced fluids often dominate and that they are efficiently channeled along fault block interfaces. Moreover, our study constrains the degree of mixing of fluid reservoirs and their relative volumetric contributions.

Rather than painting a simple picture of single fluid activity, or homogenous fluid migration across or along faults, our results show that fluid systems in the RM-FTB are multi-dimensional and complex. Variable mixing of fluids implies that the fluid regime in the fold-thrust belt was an open system, allowing the introduction, movement, and mixing of different fluids throughout ongoing deformation, focused along active thrust faults toward the front and foreland of the mountain range.

**Figure 4.** Series of cross-plots examining fluid isotopic signatures through time and with respect to position in the RM-FTB. A and B show the relation of timing of in-sequence fault slip to  $\delta^{18}O$  and  $\delta D$  of fault fluids. Fault ages from Paná and van der Pluijm (2015) and van der Pluijm et al. (2006). Plots C and D show isotopic composition with respect to latitude. Plots E and F compare isotopic composition to their relative positions in the FTB. The latter is expressed as a fractional distance across the belt, with 0 corresponding to the Southern Rocky Mountain Trench (SMRT) and 1 to the Approximate Limit of Cordillerian Deformation (LCD) (both shown in Figure 1). The width is the measured distance from the SMRT to the LCD, perpendicular to the strike of the belt through each sample location. Error is estimated to be  $\pm 0.1$ . Considering error and uncertainty, there is no correlation between any of the variables explored and fluid isotopic composition.

## Data Availability Statement

Data sets for this research are additionally available via “Deep Blue,” the University of Michigan’s data repository: Lynch and van der Pluijm (2021), [CCO 1.0, doi:10.7302/6emc-9f49].

## Acknowledgments

This project was supported by a Rackham Graduate School Predoctoral Fellowship to Lynch. Field and analytical support were provided by AER/Alberta Geological Survey. Support for clay research at the University of Michigan was provided by the National Science Foundation (most recently EAR-1629805). The authors thank Torsten Vennemann and Benita Putlitz for invaluable help and guidance in the stable isotope laboratory at UNIL. Thanks are also extended to Randy Williams, Mark Evans, and two anonymous reviewers, whose questions and contributions greatly improved and focused this article.

## References

- Anastasio, D. J., Bebout, G. E., & Holl, J. E. (2004). Extra-basinal fluid infiltration, mass transfer, and volume strain during folding: Insights from the Idaho-Montana thrust belt. *American Journal of Science*, 304(4), 333–369. <https://doi.org/10.2475/ajs.304.4.333>
- Bebout, G. E., Anastasio, D. J., & Holl, J. E. (2001). Synorogenic crustal fluid infiltration in the Idaho-Montana thrust belt. *Geophysical Research Letters*, 28(22), 4295–4298. <https://doi.org/10.1029/2001GL013711>
- Boles, A., van der Pluijm, B., Mulch, A., Mutlu, H., Uysal, T., & Warr, L. (2015). Hydrogen and  $^{40}\text{Ar}/^{39}\text{Ar}$  isotope evidence for multiple and protracted paleofluid flow events within the long-lived North Anatolian Keirogen (Turkey). *Geochemistry, Geophysics, Geosystems*, 16(6), 1975–1987. <https://doi.org/10.1002/2015GC005810>
- Bowen, G. J., & Revenaugh, J. (2003). Interpolating the isotopic composition of modern meteoric precipitation. *Water Resources Research*, 39(10). <https://doi.org/10.1029/2003WR002086>
- Bradbury, H. J., & Woodwell, G. R. (1987). Ancient fluid flow within foreland terrains. *Geological Society, London, Special Publications*, 34, 87–102. <https://doi.org/10.1144/GSL.SP.1987.034.01.07>
- Capuano, R. (1992). The temperature dependence of hydrogen isotope fractionation between clay minerals and water: Evidence from a geopressured system. *Geochimica et Cosmochimica Acta*, 56, 2547–2554. [https://doi.org/10.1016/0016-7037\(92\)90208-Z](https://doi.org/10.1016/0016-7037(92)90208-Z)
- Chamberlain, C. P., Mix, H. T., Mulch, A., Hren, M. T., Kent-Corson, M. L., Davis, S. J., et al. (2012). The Cenozoic climatic and topographic evolution of the western North American Cordillera. *American Journal of Science*, 312(2), 213–262. <https://doi.org/10.2475/02.2012.05>
- Connolly, C. A., Walter, L. M., Baadsgaard, H., & Longstaffe, F. J. (1990). Origin and evolution of formation waters, Alberta Basin, Western Canada sedimentary basin. II. Isotope systematics and water mixing. *Applied Geochemistry*, 5(4), 397–413. [https://doi.org/10.1016/0883-2927\(90\)90017-Y](https://doi.org/10.1016/0883-2927(90)90017-Y)
- Cooley, M. A., Price, R. A., Kyser, T. K., & Dixon, J. M. (2011). Stable-isotope geochemistry of syntectonic veins in Paleozoic carbonate rocks in the Livingstone Range anticlinorium and their significance to the thermal and fluid evolution of the southern Canadian foreland thrust and fold belt. *AAPG Bulletin*, 95(11), 1851–1882. <https://doi.org/10.1306/01271107098>
- Dworkin, S. I. (1999). Geochemical constraints on the origin of thrust fault fluids. *Geophysical Research Letters*, 26(24), 3665–3668. <https://doi.org/10.1029/1999GL008377>
- England, T. D. J., & Bustin, R. M. (1986). Effect of thrust faulting on organic maturation in the southeastern Canadian Cordillera. *Organic Geochemistry*, 10(1–3), 609–616. [https://doi.org/10.1016/0146-6380\(86\)90057-4](https://doi.org/10.1016/0146-6380(86)90057-4)
- Evans, J. P., Forster, C. B., & Goddard, J. V. (1997). Permeability of fault-related rocks, and implications for hydraulic structure of fault zones. *Journal of Structural Geology*, 19(11), 1393–1404. [https://doi.org/10.1016/S0191-8141\(97\)00057-6](https://doi.org/10.1016/S0191-8141(97)00057-6)
- Evans, M. A., & Battles, D. A. (1999). Fluid inclusion and stable isotope analyses of veins from the central Appalachian Valley and Ridge province: Implications for regional synorogenic hydrologic structure and fluid migration. *Geological Society of America Bulletin*, 111(12), 1841–1860. [https://doi.org/10.1130/0016-7606\(1999\)111<1841:FIASIA>2.3.CO;2](https://doi.org/10.1130/0016-7606(1999)111<1841:FIASIA>2.3.CO;2)
- Evans, M. A., Bebout, G. E., & Brown, C. H. (2012). Changing fluid conditions during folding: An example from the central Appalachians. *Tectonophysics*, 576–577, 99–115. <https://doi.org/10.1016/j.tecto.2012.03.002>
- Evenchick, C. A., McMechan, M. E., McNicoll, V. J., & Carr, S. D. (2007). A synthesis of the Jurassic-Cretaceous tectonic evolution of the central and southeastern Canadian Cordillera: Exploring links across the orogen. In L. W. Sears, T. A. Harms, & C. A. Evenchick (Eds.), *Whence the mountains? Inquiries into the evolution of an orogenic system: A volume in honor of Raymore A. Price: GSA Special Paper* (Vol. 443, pp. 117–145). [https://doi.org/10.1130/2007.2433\(06\)10.1130/2007.2433\(06\)](https://doi.org/10.1130/2007.2433(06)10.1130/2007.2433(06))
- Faulkner, D. R., & Armitage, P. J. (2013). The effect of tectonic environment on permeability development around faults and in brittle crust. *Earth and Planetary Science Letters*, 375, 71–77. <https://doi.org/10.1016/j.epsl.2013.05.006>
- Faulkner, D. R., Jackson, C. A. L., Lunn, R. J., Schlische, R. W., Shipton, Z. K., Wibberley, C. A. J., & Withjack, M. O. (2010). A review or recent developments concerning the structure, mechanics, and fluid flow properties of fault zones. *Journal of Structural Geology*, 32, 1557–1575. <https://doi.org/10.1016/j.jsg.2010.06.009>
- Fitz-Diaz, E., Camprubi, A., Cienfuegos-Alvarado, E., Morales-Puente, P., Schleicher, A. M., & van der Pluijm, B. A. (2014). Newly formed illite preserves fluid sources during folding of shale and limestone rocks; an example from the Mexican fold-thrust belt. *Earth and Planetary Science Letters*, 391, 263–273. <https://doi.org/10.1016/j.epsl.2013.12.025>
- Fitz-Diaz, E., Hudleston, P., Siebenaller, L., Kirschner, D. L., Camprubi, A., Tolson, G., & Puig, T. P. (2011). Insights into fluid flow and water-rock interaction during deformation of carbonate sequences in the Mexican fold-thrust belt. *Journal of Structural Geology*, 33(8), 1237–1253. <https://doi.org/10.1016/j.jsg.2011.05.009>
- Fyfe, W. S., & Kerrich, R. (1985). Fluids and thrusting. *Chemical Geology*, 49(1–3), 353–362. [https://doi.org/10.1016/0009-2541\(85\)90167-6](https://doi.org/10.1016/0009-2541(85)90167-6)
- Gabrielse, H., Monger, J. W. H., Wheeler, J. O., & Yorath, C. J. (1992). Morphogeological belts, tectonic assemblages, and terranes: Chapter 2, Part A. In H. Gabrielse, & C. J. Yorath (Eds.), *Geology of the Cordilleran Orogen in Canada. Geological Survey of Canada, Geology of Canada*, 4 (pp. 15–28). Geological Society of America, The Geology of North America. <https://doi.org/10.4095/134073>
- Ge, S., & Garven, G. (1989). Tectonically induced transient groundwater flow in foreland basin. *Geophysical Monograph Series*, 14(3), 145–157. <https://doi.org/10.1029/GM048p0145>
- Haines, S., Lynch, E. A., Mulch, A., Valley, J. W., & van der Pluijm, B. A. (2016). Meteoric fluid infiltration in crustal-scale normal fault systems as indicated by  $\delta^{18}\text{O}$  and  $\delta^2\text{H}$  geochemistry and  $^{40}\text{Ar}/^{39}\text{Ar}$  dating of neofomed clays in brittle fault rocks. *Lithosphere*, 8(6), 587–600. <https://doi.org/10.1130/L483.1>
- Haines, S., & van der Pluijm, B. (2012). Patterns of mineral transformations in clay gouge, with examples from low-angle normal fault rocks in the western USA. *Journal of Structural Geology*, 43, 2–32. <https://doi.org/10.1016/j.jsg.2012.05.004>
- Hardebol, N. J., Callot, J. P., Bertotti, G., & Faure, J. L. (2009). Burial and temperature evolution in thrust belt systems: Sedimentary and thrust sheet loading in the SE Canadian Cordillera. *Tectonics*, 28(3). <https://doi.org/10.1029/2008TC002335>
- Hitchon, B., & Friedman, I. (1969). Geochemistry and origin of formation waters in the Western Canada sedimentary basin—I. Stable isotopes of hydrogen and oxygen. *Geochimica et Cosmochimica Acta*, 33(11), 1321–1349. [https://doi.org/10.1016/0016-7037\(69\)90178-1](https://doi.org/10.1016/0016-7037(69)90178-1)

- Hüpers, A., Torres, M. E., Owari, S., McNeill, L. C., Dugan, B., Henstock, T. J., et al. (2017). Release of mineral-bound water prior to subduction tied to shallow seismogenic slip off Sumatra. *Science*, 356(6340), 841–844. <https://doi.org/10.1126/science.aal3429>
- Kalkreuth, W., & McMechan, M. E. (1984). Regional pattern of thermal maturation as determined from coal-rank studies, Rocky Mountain Foothills and Front Ranges north of Grande Cache, Alberta—Implications for petroleum exploration. *Bulletin of Canadian Petroleum Geology*, 32(3), 249–271. <https://doi.org/10.35767/gscpgbull.32.3.249>
- Kirschner, D. L., & Kennedy, L. A. (2001). Limited syntectonic fluid flow in carbonate-hosted thrust faults of the Front Ranges, Canadian Rockies, inferred from stable isotope data and structures. *Journal of Geophysical Research*, 106(B5), 8827–8840. <https://doi.org/10.1029/2000JB900414>
- Koons, P. O., & Craw, D. (1991). Evolution of fluid driving forces and composition within collisional orogens. *Geophysical Research Letters*, 18(5), 935–938. <https://doi.org/10.1029/91GL00910>
- Longstaffe, F. J., & Ayalon, A. (1990). Hydrogen-isotope geochemistry of diagenetic clay minerals from Cretaceous sandstones, Alberta, Canada: Evidence for exchange. *Applied Geochemistry*, 5(5), 657–668. [https://doi.org/10.1016/0883-2927\(90\)90063-B](https://doi.org/10.1016/0883-2927(90)90063-B)
- Lynch, E. A., Mulch, A., Yonkee, A., & van der Pluijm, B. (2019). Surface fluids in the evolving Sevier fold-thrust belt of ID-WY indicated by hydrogen isotopes in dated, authigenic clay minerals. *Earth and Planetary Science Letters*, 513, 29–39. <https://doi.org/10.1016/j.epsl.2019.02.003>
- Lynch, E. A., & van der Pluijm, B. (2016). Meteoric fluid infiltration in the Argentine Precordillera fold-and-thrust belt: Evidence from H isotopic studies of neofomed clay minerals. *Lithosphere*, 9(1), 134–145. <https://doi.org/10.1130/L568.1>
- Lynch, E. A., & van der Pluijm, B. (2021). *Canadian Cordillera Fault Gouge XRD and isotopes [Data set]*. University of Michigan—Deep Blue Data.
- Machel, H. G., & Cavell, P. A. (1999). Low-flux, tectonically induced squeeze fluid flow (“hot flash”) into the Rocky Mountain foreland basin. *Bulletin of Canadian Petroleum Geology*, 47(4), 510–533. <https://doi.org/10.35767/gscpgbull.47.4.510>
- Menzies, C., Teagle, D., Craw, D., Cox, S., Boyce, A., Barrie, C., & Roberts, S. (2014). Incursion of meteoric waters into the ductile regime in an active orogen. *Earth and Planetary Science Letters*, 399, 1–13. <https://doi.org/10.1016/j.epsl.2014.04.046>
- Menzies, C. D., Teagle, D. A. H., Niedermann, S., Cox, S. C., Craw, D., Zimmer, M., et al. (2016). The fluid budget of a continental plate boundary fault: Quantification from the Alpine Fault, New Zealand. *Earth and Planetary Science Letters*, 445, 125–135. <https://doi.org/10.1016/j.epsl.2016.03.046>
- Monger, J. W. H. (1984). Cordilleran tectonics: A Canadian perspective. *Bulletin of the Geological Society of France*, S7-XXVI(2), 255–278. <https://doi.org/10.2113/gssgfbull.S7-XXVI.2.255>
- Monger, J. W. H. (1989). Overview of Cordilleran geology; Chapter 2. In B. D. Ricketts (Ed.), *Western Canada sedimentary basin: A case history* (pp. 9–32). Canadian Society of Petroleum Geologists.
- Monger, J. W. H., Gabrielse, H., & Souther, J. G. (1972). Evolution of the Canadian Cordillera: A plate-tectonic model. *American Journal of Science*, 272, 577–602. <https://doi.org/10.2475/ajs.272.7.577>
- Monger, J. W. H., & Gibson, H. D. (2019). Mesozoic-Cenozoic deformation in the Canadian Cordillera: The record of a “Continental Bulldozer”? *Tectonophysics*, 757, 153–169. <https://doi.org/10.1016/j.tecto.2018.12.023>
- Monger, J. W. H., & Price, R. A. (2002). The Canadian Cordillera: Geology and tectonic evolution. *Canadian Society of Exploration Geophysicists, Recorder*, 17–36.
- Monger, J. W. H., Price, R. A., & Tempelman-Kluit, D. J. (1982). Tectonic accretion and the origin of two major metamorphic and plutonic belts in the Canadian Cordillera. *Geology*, 10, 70–75. [https://doi.org/10.1130/0091-7613\(1982\)10<70:taatoo>2.0.co;2](https://doi.org/10.1130/0091-7613(1982)10<70:taatoo>2.0.co;2)
- Moore, D. M., & Reynolds, R. C., Jr. (1997). *X-ray diffraction and the identification and analysis of clay minerals*. Oxford University Press.
- Nesbitt, B. E., & Muehlenbachs, K. (1989). Geology, Geochemistry, and Genesis of Mesothermal Lode Gold Deposits of the Canadian Cordillera: Evidence for ore formation from evolved meteoric water. In R. R. Keays, W. Ramsay, & D. I. Groves (Eds.), *Economic Geology Monograph Series* (Vol. 6, pp. 553–563). <https://doi.org/10.5382/Mono.06.42>
- Nesbitt, B. E., & Muehlenbachs, K. (1991). Stable isotopic constraints on the nature of the syntectonic fluid regime of the Canadian Cordillera. *Geophysical Research Letters*, 18(5), 963–966. <https://doi.org/10.1029/91GL00914>
- Nesbitt, B. E., & Muehlenbachs, K. (1994). Paleohydrogeology of the Canadian Rockies and origins of brines, Pb-Zn deposits and dolomitization in the Western Canada sedimentary basin. *Geology*, 22(3), 243–246. [https://doi.org/10.1130/0091-7613\(1994\)022<0243:POTCRA>2.3.CO;2](https://doi.org/10.1130/0091-7613(1994)022<0243:POTCRA>2.3.CO;2)
- Nesbitt, B. E., & Muehlenbachs, K. (1995). Geochemical studies of the origins and effects of synorogenic crustal fluids in the southern Omineca Belt of British Columbia, Canada. *GSA Bulletin*, 107, 1033–1050. [https://doi.org/10.1130/0016-7606\(1995\)107<1033:GSOTOA>2.3.CO;2](https://doi.org/10.1130/0016-7606(1995)107<1033:GSOTOA>2.3.CO;2)
- Osadetz, K. G., Kohn, B. P., Feinstein, S., & Price, R. A. (2004). Foreland belt thermal history using apatite fission-track thermochronology: Implications for Lewis thrust and Flathead fault in the southern Canadian Cordilleran petroleum province. In R. Swennen, F. Roure, & J. W. Granath (Eds.), *Deformation, fluid flow, and reservoir appraisal in foreland fold and thrust belts, AAPG Hedberg Series* (Vol. 1, pp. 21–48). <https://doi.org/10.1306/1025684H13111>
- Paná, D. I., & Elgr, R. (2013). *Geological map of the Alberta Rocky Mountains and Foothills (NTS 82G, 82H, 82I, 82O, 82N, 83B, 83C, 83D, 83F, 83E, and 83L)*. (Map 560, scale 1:500,000). Energy Resources Conservation Board (ERCB)/Alberta Geological Survey (AGS). Retrieved from <http://www.ags.gov.ab.ca/publications/MAP/PDF/MAP560.PDF>
- Paná, D. I., & van der Pluijm, B. A. (2015). Orogenic pulses in the Alberta Rocky Mountains: Radiometric dating of major faults and comparison with the regional tectono-stratigraphic record. *Geological Society of America Bulletin*, 127(3–4), 480–502. <https://doi.org/10.1130/B31069.1>
- Price, R. A. (1981). The Cordilleran foreland thrust and fold belt in the southern Canadian Rocky Mountains. *Geological Society, London, Special Publications*, 9(1), 427–448. <https://doi.org/10.1144/gsl.sp.1981.009.01.39>
- Price, R. A. (1986). The southeastern Canadian Cordillera: Thrust faulting, tectonic wedging, and delamination of the lithosphere. *Journal of Structural Geology*, 8, 239–254. [https://doi.org/10.1016/0191-8141\(86\)90046-5](https://doi.org/10.1016/0191-8141(86)90046-5)
- Price, R. A. (1994). Cordilleran tectonics and the evolution of the Western Canada sedimentary basin. In G. Mossop, & I. Shetsen (Eds.), *Geological Atlas of the Western Canada sedimentary basin* (pp. 13–24). Canadian Society of Petroleum Geologists and Alberta Research Council.
- Ross, G. M., & Villeneuve, M. (2003). Provenance of the Mesoproterozoic (1.45 Ga) Belt basin (western North America): Another piece in the pre-Rodinia paleogeographic puzzle. *Geological Society of America Bulletin*, 115(10), 1191–1217. <https://doi.org/10.1130/B25209.1>
- Rygel, A. C., Anastasio, D. J., & Bebout, G. E. (2006). Syntectonic infiltration by meteoric waters along the Sevier thrust front, southwest Montana. *Geofluids*, 6(4), 288–301. <https://doi.org/10.1111/j.1468-8123.2006.00146.x>
- Sears, J. W., & Price, R. A. (2003). Tightening the Siberian connection to western Laurentia. *Geological Society of America Bulletin*, 115, 227–953. <https://doi.org/10.1130/B25229.1>



- Sharp, Z. D. (1990). A laser-based microanalytical method for the in situ determination of oxygen isotope ratios of silicates and oxides. *Geochimica et Cosmochimica Acta*, 54(5), 1353–1357. [https://doi.org/10.1016/0016-7037\(90\)90160-M](https://doi.org/10.1016/0016-7037(90)90160-M)
- Sheppard, S., & Gilg, H. (1996). Stable isotope geochemistry of clay minerals. *Clay Minerals*, 31(1), 1–24. <https://doi.org/10.1180/claymin.1996.031.1.01>
- Sheppard, S. M. F. (1986). Characterization and isotopic variations in natural waters. *Reviews in Mineralogy and Geochemistry*, 16(1), 165–184. <https://doi.org/10.1515/9781501508936-011>
- Sibson, R. H. (1992). Fault-valve behavior and the hydrostatic-lithostatic fluid pressure interface. *Earth-Science Reviews*, 32(1), 141–144. [https://doi.org/10.1016/0012-8252\(92\)90019-P](https://doi.org/10.1016/0012-8252(92)90019-P)
- Struik, L. C. (1988). Crustal evolution of the eastern Canadian Cordillera. *Tectonics*, 7, 727–747. <https://doi.org/10.1029/tc007i004p00727>
- Symons, D. T. A., & Cioppa, M. T. (2002). Conodont CAI and magnetic mineral unblocking temperatures: Implications for the Western Canada sedimentary basin. *Physics and Chemistry of the Earth*, 27(25–31), 1189–1193. [https://doi.org/10.1016/S1474-7065\(02\)00129-8](https://doi.org/10.1016/S1474-7065(02)00129-8)
- Tempelman-Kluit, D. J. (1979). *Transported Cataclasite, Ophiolite, and Granodiorite in Yukon: Evidence of arc-continent collision*. Geological Survey of Canada Paper.
- Travé, A., Labaume, P., & Verges, J. (2007). Fluid systems in foreland fold-and-thrust belts: An overview from the Southern Pyrenees. In O. Lacombe, J. Lave, F. Roure, & J. Verges (Eds.), *Thrust belts and foreland basins: From fold kinematics to hydrocarbon systems* (pp. 99–115). Springer. [https://doi.org/10.1007/978-3-540-69426-7\\_5](https://doi.org/10.1007/978-3-540-69426-7_5)
- van der Pluijm, B. A., Hall, C. M., Vrolijk, P., Pevear, D. R., & Covey, M. C. (2001). The dating of shallow faults in the Earth's crust. *Nature*, 412, 172–175. <https://doi.org/10.1038/35084053>
- van der Pluijm, B. A., Vrolijk, P., Pevear, D. R., Hall, C. M., & Solum, J. G. (2006). Fault dating in the Canadian Rocky Mountains: Evidence for late Cretaceous and early Eocene orogenic pulses. *Geology*, 34(10), 837–840. <https://doi.org/10.1130/G22610.1>
- Walther, J. V., & Wood, B. J. (1984). Rate and mechanism in prograde metamorphism. *Contributions to Mineralogy and Petrology*, 88(3), 246–259. <https://doi.org/10.1007/BF00380169>
- York, D. (1968). Least squares fitting of a straight line with correlated errors. *Earth and Planetary Science Letters*, 5, 320–324. [https://doi.org/10.1016/s0012-821x\(68\)80059-7](https://doi.org/10.1016/s0012-821x(68)80059-7)